IOP PUBLISHING INVERSE PROBLEMS

Inverse Problems **24** (2008) 065016 (15pp) doi:10.1088/0266-5611/24/6/065016

Transmission eigenvalues and the nondestructive testing of dielectrics

Fioralba Cakoni[1], **Mehmet Çayören**[2] **and David Colton**[1]

[1] Department of Mathematical Sciences, University of Delaware, Newark, DE 19716, USA
[2] Istanbul Technical University, Electrical and Electronics Engineering Faculty, 34469 Maslak, Istanbul, Turkey

E-mail: cakoni@math.udel.edu, mehmet@cayoren.com and colton@math.udel.edu

Received 24 June 2008, in final form 3 September 2008
Published 6 November 2008
Online at stacks.iop.org/IP/24/065016

Abstract

We show how transmission eigenvalues can be determined from electromagnetic scattering data and used to determine the presence of cavities in a dielectric.

(Some figures in this article are in colour only in the electronic version)

1. Introduction

In this paper we would like to suggest a new method for nondestructive testing of dielectrics. This method is based on determining transmission eigenvalues from electromagnetic scattering data and deducing the presence of cavities in the dielectric from the location of the eigenvalues. The model problem we have in mind (although many others are possible!) is the location of cavities in tree trunks, which for E-polarized electromagnetic waves polarized parallel to the axis of the tree trunk, the scattering problem can be modeled by the Helmholtz equation with variable permittivity (note that, since wood is orthotropic, H-polarized waves would lead to a different equation to the Helmholtz equation).

Transmission eigenvalues have appeared only recently in the world of scattering theory and for an introduction to this unusual spectral problem in partial differential equations we refer the reader to sections 8.4 and 8.6 of [6] and the survey paper [7]. In [1] it was shown that, under the assumption that the relative permittivity ϵ_r was greater than one, transmission eigenvalues could be determined from scattering data and used to give a lower bound for ϵ_r. In the present paper we will encounter a transmission eigenvalue problem that has not been considered before, i.e. the case when $\epsilon_r = 1$ in a portion D_0 of the scattering obstacle D. In particular D_0 corresponds to the location of cavities in the obstacle. We will provide numerical evidence showing that the presence of a nonempty cavity $D_0 \subset D$ causes the transmission eigenvalues to increase with the magnitude of the increase depending on the size of D_0. Although we have been unable to prove this fact analytically, we will establish in

the following section that this relationship does hold asymptotically. We draw attention to the fact that in this paper we are primarily considering the simple scattering problem where the incident field is a time harmonic plane wave and the measured data are far field data. The more realistic problem of point source as incident fields and near field scattering data can be handled in the same way by measuring both the electric and magnetic fields and using the reciprocity gap functional instead of the far field operator to determine the transmission eigenvalues. We will discuss this problem in section 3 of this paper.

The plan of our paper is as follows. In the following section, we formulate the direct scattering problem for electromagnetic waves by a dielectric inhomogeneous infinite cylinder with cross section D having cavities with cross section $D_0 \subset D$ such that in D_0 we have $\epsilon_r = 1$. We will establish that as either $\epsilon_r \to 1$ or area $(D\backslash D_0) \to 0$ the transmission eigenvalues tend to infinity (in particular, this implies that in the Born approximation transmission eigenvalues do not exist—see also [7]). We then consider the case of near field data. We conclude by presenting a number of numerical examples that indicate that amount of the shift of the transmission eigenvalues due to the presence of a cavity depends on the size of the cavity or, if the same size, how near the surface the cavity is. We also present evidence that this shift can also be detected even if the scattering obstacle has a moderate amount of absorption.

2. Scattering by a cylinder and transmission eigenvalues

We consider the scattering of a time harmonic electromagnetic plane wave by an inhomogeneous dielectric infinite cylinder with cross section D such that the electric field $E = (0, 0, u\,\mathrm{e}^{-\mathrm{i}\omega t})$ is polarized parallel to the axis of the cylinder. Thus, assuming that the relative permittivity is independent of the position along the axis of the cylinder, and factoring out the harmonic term $\mathrm{e}^{-\mathrm{i}\omega t}$, $u = u(x)$ satisfies [6]

$$\Delta u + k^2 \epsilon_r(x) u = 0 \qquad \text{in} \quad \mathbb{R}^2, \tag{1}$$

$$u(x) = \mathrm{e}^{\mathrm{i}kx\cdot d} + u^s(x) \qquad \text{in} \quad \mathbb{R}^2, \tag{2}$$

$$\lim_{r\to\infty} \sqrt{r}\left(\frac{\partial u^s}{\partial r} - \mathrm{i}ku^s\right) = 0, \tag{3}$$

where $x \in \mathbb{R}^2$, $r = |x|$, $k > 0$ is the wave number, d is a vector on the unit circle S in $\mathbb{R}^2$ and the Sommerfeld radiation condition (3) is assumed to hold uniformly with respect to $\hat{x} = x/|x|$. The relative permittivity $\epsilon_r = \epsilon_r(x)$ is required to be a piecewise continuously differentiable function with jumps along piecewise smooth curves ∂D_0 bounding a region D_0 such that $\epsilon_r(x) = 1$ in $\mathbb{R}^2\backslash\overline{D}$ and D_0 and $\epsilon_r(x) > 1$ in $\overline{D}\backslash\overline{D}_0$ where $\overline{D}$ is compact, the complement of D is connected and $D\backslash\overline{D}_0$ has piecewise smooth boundary with unit outward normal ν. (D_0 can be the empty set. The region D_0 represents the possibly multiply connected portion of D in which there is a cavity.) Without loss of generality we assume that $D\backslash\overline{D}_0$ contains the origin.

The existence of a unique solution $u \in H^1_{\mathrm{loc}}(\mathbb{R}^2)$ to (1)–(3) can be established by either variational methods or the use of integral equations [6]. It can be shown that the scattered field u^s has the asymptotic behavior

$$u^s(x) = \frac{\mathrm{e}^{\mathrm{i}kr}}{\sqrt{r}} u_\infty(\hat{x}; d, k) + O(r^{-3/2}) \tag{4}$$

as $r \to \infty$ uniformly in $\hat{x}$ where u_∞ is the far field pattern of the scattered field u^s. Given the far field pattern, we can now define the *far field operator* $F : L^2(S) \to L^2(S)$ by

$$(Fg)(\hat{x}) := \int_S u_\infty(\hat{x}; d, k) g(d)\, \mathrm{d}s_d. \tag{5}$$

We note that $(Fg)(\hat{x})$ is the far field corresponding to (1)–(3) where the incident field $e^{ikx\cdot d}$ is replaced by the *Herglotz wavefunction*

$$v_g(x) := \int_S e^{ikx\cdot d} g(d)\, ds_d. \tag{6}$$

The following theorem is a reformulation and slight strengthening of theorem 8.9 of [6].

Theorem 2.1. *The far field operator is injective with dense range if and only if there does not exist a solution* $v, w \in L^2(D)$, $v-w \in H^2(D)$ *of the interior transmission problem*

$$\Delta w + k^2 \epsilon_r(x) w = 0 \qquad in \quad D, \tag{7}$$

$$\Delta v + k^2 v = 0 \qquad in \quad D, \tag{8}$$

$$w = v \qquad on \quad \partial D, \tag{9}$$

$$\frac{\partial w}{\partial \nu} = \frac{\partial v}{\partial \nu} \qquad on \quad \partial D, \tag{10}$$

such that v *is a Herglotz wavefunction.*

Values of k such that there exists a nontrivial solution of the interior transmission problem are called *transmission eigenvalues*. If $\epsilon_r(x) > 1 + \sigma$ for $x \in D$ and a positive constant $\sigma > 0$, and $D_0 = \emptyset$ it is known that transmission eigenvalues exist and they form a discrete set [7, 8]. In our problem $\epsilon_r(x) = 1$ for $x \in D_0 \subset D$ where D_0 is in general not the empty set and these results no longer apply. However, assuming that transmission eigenvalue exists, we can prove the following theorem which is the main result of the section (see [9] for estimates of a similar nature).

Theorem 2.2. *Let* k *be a transmission eigenvalue. If either (a)* $\sup_{D\setminus\overline{D}_0} \epsilon_r(x) \to 1$ *or (b) the area of* $(D\setminus\overline{D}_0) \to 0$ *then* $k \to \infty$.

Proof. Assume that k is a transmission eigenvalue and let $v, w \in H^1(D)$ be a nontrivial solution of (7)–(10). Then from Green's formula v and w satisfy the integral equation

$$v = w - k^2 T w, \tag{11}$$

where

$$(Tf)(x) := \frac{i}{4} \int_{D\setminus D_0} H_0^{(1)}(k|x-y|) m(y) f(y)\, dy,$$

$m = \epsilon_r - 1$ and $H_0^{(1)}$ is a Hankel function of the first kind of order zero. Note that from (7)–(10) we see that Tf can be continued as a radiating solution of (7) into $\mathbb{R}^2\setminus D$ such that $Tf = 0$ in $\mathbb{R}^2\setminus D$ and hence letting $|x| \to \infty$ we have that

$$\int_{D\setminus D_0} e^{-ik\hat{x}\cdot y} m(y) w(y)\, dy = 0, \qquad \hat{x} \in S. \tag{12}$$

Now let

$$L^2_m(D\setminus D_0) := \left\{ u : u \text{ measurable}, \int_{D\setminus D_0} m(x)|u(x)|^2\, dx < \infty \right\}$$

and let $\|\cdot\|_m$ be the corresponding norm in $L^2_m(D\setminus D_0)$. Let

$$H := \text{span}\{J_n(kr)\, e^{in\theta} : n = 0, \pm 1, \pm 2, \ldots\} \tag{13}$$

where J_n is a Bessel function of order n and let $\overline{H}$ denote the closure of H in $L^2_m(D\backslash D_0)$. Then from (12) and the Jacobi–Anger expansion we see that $w \in H^\perp$ and hence if $P : L^2_m(D\backslash D_0) \to H^\perp$ is the projection operator of $L^2_m(D\backslash D_0)$ onto $H^\perp$ we have from (11) that

$$0 = w + k^2 PTw.$$

It follows that if k is a transmission eigenvalue then $k^2\|T\|_m > 1$.

We now estimate $\|T\|_m$. To this end we have that

$$\begin{aligned}
|(Tf)(x)|^2 &= \left|\frac{\mathrm{i}}{4}\int_{D\backslash D_0} H_0^{(1)}(k|x-y|)m(y)f(y)\,\mathrm{d}y\right|^2 \\
&\leqslant \frac{1}{4}\int_{D\backslash D_0}\left|H_0^{(1)}(k|x-y|)\right|^2 m(y)\,\mathrm{d}y \int_{D\backslash D_0} m(y)|f(y)|^2\,\mathrm{d}y \\
&\leqslant \frac{M}{4}\left[\int_D \left|H_0^{(1)}(k|x-y|)\right|^4 \mathrm{d}y\right]^{1/2} [\mathrm{area}(D\backslash D_0)]^{1/2}\,\|f\|_m \\
&\leqslant C(1+|\log k|)^2(\mathrm{area}(D\backslash D_0))^{1/2}\|f\|_m,
\end{aligned}$$

where $M := \sup_{D\backslash D_0} m(x)$ and $C > 0$ is a constant independent of m, D_0 and k such that

$$\sup_D \frac{1}{4}\left[\int_D \left|H_0^{(1)}(k|x-y|)\right|^4 \mathrm{d}y\right]^{1/2} < C(1+|\log k|)^2.$$

The fact that such a constant C exists and is independent of m, D_0 and k follows from lemma 2.4 of [1]. We now have that

$$\|Tf\|_m^2 = \int_{D\backslash D_0} m|Tf|^2\,\mathrm{d}x \leqslant CM^2(1+|\log k|)^2(\mathrm{area}(D\backslash D_0))^{3/2}\|f\|_m,$$

i.e.

$$\|T\|_m \leqslant CM^2(1+|\log k|)^2(\mathrm{area}(D\backslash D_0))^{3/2}$$

and the theorem follows. □

The proof of the above theorem shows that if k is a transmission eigenvalue, i.e. $v, w \in H^1(D)$ is a nontrivial solution of (7)–(10), then v can be approximated in $L^2_m(D\backslash D_0)$ by an element of H, in particular a Herglotz wavefunction. But from theorem 2.1 the far field operator is not injective when k is a transmission eigenvalue and v is a Herglotz function. Hence, since we are assuming that $D\backslash\overline{D}_0$ contains the origin, we can expect as in [1] that the norm of the regularized solution $g \in L^2(S)$ of

$$(F(g))(\hat{x}) = 1 \tag{14}$$

will be large if k is a transmission eigenvalue. Although we cannot prove this, the numerical examples given in section 4 support this expectation and the above procedure thus provides a heuristic method for determining the transmission eigenvalues from far field data. These same numerical examples indicate that the transmission eigenvalues increase when a cavity D_0 is present and that the size of the increase depends on the size of D_0. Again, we cannot prove that this observed behavior is in fact always true except for the limiting case of part (b) of theorem 2.2.

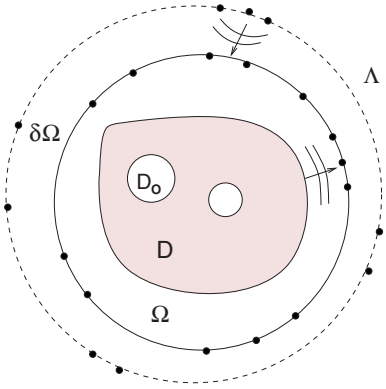

Figure 1. Configuration with near field measurements.

3. Near field data

In nondestructive testing problems the object is typically interrogated by using point sources as incident waves and the total field is measured near the scatterer. In this section we show that the ideas introduced in section 2 can be applied to the case of near field measurements, in which case the far field equation is replaced by an equation based on the reciprocity gap functional [4]. To treat near field data we could of course use the far field equation (14) with u_∞ replaced by u^s measured on a curve outside D and the right-hand side replaced by $H_0^{(1)}(k|x|)$. However, this approach assumes a homogeneous background whereas the gap reciprocity approach that we use in this section does not assume this. In particular, due to the fact that both the electric and magnetic fields are used, the presence of the antenna and other objects in the exterior of the measurement surface does not affect the proposed inversion procedure. The main results of this section show that the reciprocity gap operator exhibits similar properties as the far field operator.

Assuming that ϵ_r satisfies the properties stated at the beginning of section 2, the total field $u(x; x_0)$ now satisfies

$$\Delta u(x; x_0) + k^2 \epsilon_r(x) u(x; x_0) = 0 \qquad \text{in} \quad \mathbb{R}^2 \backslash \{x_0\}, \tag{15}$$

$$u(x; x_0) = \Phi(x; x_0) + u^s(x; x_0) \qquad \text{in} \quad \mathbb{R}^2, \tag{16}$$

$$\lim_{r\to\infty} \sqrt{r}\left(\frac{\partial u^s}{\partial r} - \mathrm{i}k u^s\right) = 0, \tag{17}$$

where $u^s(\cdot; x_0) \in H^1_{loc}(\mathbb{R}^2)$ is the scattered field due to the obstacle D, $\Phi(x; x_0) = \frac{\mathrm{i}}{4} H_0^{(1)}(k|x - x_0|)$ is a point source located at $x_0 \in \mathbb{R}^2 \backslash \overline{D}$ and the Sommerfeld radiation condition (17) is again assumed to hold uniformly with respect to $\hat{x} = x/|x|$.

We now suppose that we know $u(\cdot; x_0)$ and $\frac{\partial u(\cdot; x_0)}{\partial \nu}$ on $\partial\Omega$ for all $x_0 \in \Lambda$ where $\partial\Omega$ and Λ are two smooth closed curves such that $\partial\Omega$ is the boundary of the open region Ω containing $\overline{D}$ inside whereas Λ is the boundary of a bounded domain containing $\overline{\Omega}$ in the interior. (Note that Λ can also be only part of an analytic closed curve surrounding $\overline{\Omega}$.) The configuration of the location of the receivers and transmitters is shown in figure 1.

We define

$$\mathcal{U} := \{u(x; x_0) \text{ satisfies (15)–(17) for all } x_0 \in \Lambda\}$$

and the *reciprocity gap functional* $\mathcal{R}$ on $\mathcal{U} \times \mathbb{H}(\Omega)$ by

$$\mathcal{R}(u(\cdot; x_0), v) = \int_{\partial\Omega} \left(u(\cdot; x_0) \frac{\partial v}{\partial \nu} - v \frac{\partial u(\cdot; x_0)}{\partial \nu} \right) \mathrm{d}s, \tag{18}$$

where

$$\mathbb{H}(\Omega) := \{ v \in H^1(\Omega) : \text{ such that } \Delta v + k^2 v = 0 \}.$$

We note that the integrals in (18) are interpreted in the sense of duality between $H^{1/2}(\partial\Omega)$ and $H^{-1/2}(\partial\Omega)$. Finally, we introduce the *reciprocity gap operator* $R : \mathbb{H}(\Omega) \to L^2(\Lambda)$ defined by

$$(R(v))(x_0) := \mathcal{R}(u(\cdot; x_0), v) \tag{19}$$

which is obviously a bounded and compact linear operator.

The next two theorems play a fundamental role in our method. (For the case of Maxwell's equations, see [2].)

Theorem 3.1. *The reciprocity gap operator $R : \mathbb{H}(\Omega) \to L^2(\Lambda)$ is injective if and only if k is not a transmission eigenvalue.*

Proof. Let $Rv = 0$ which means that $\mathcal{R}(u(\cdot; x_0), v) = 0$ for all $x_0 \in \Lambda$. Using Green's formulae we have

$$\begin{aligned} 0 &= \int_{\partial\Omega} \left(u(\cdot; x_0) \frac{\partial v}{\partial \nu} - v \frac{\partial u(\cdot; x_0)}{\partial \nu} \right) \mathrm{d}s \\ &= \int_{\partial D} \left(u(\cdot; x_0) \frac{\partial v}{\partial \nu} - v \frac{\partial u(\cdot; x_0)}{\partial \nu} \right) \mathrm{d}s = k^2 \int_D (\epsilon_r - 1) u(\cdot; x_0) v \, \mathrm{d}x. \end{aligned} \tag{20}$$

Now let $\tilde{w} \in H^1_{\mathrm{loc}}(\mathbb{R}^2)$ be the solution of the scattering problem

$$\Delta \tilde{w} + k^2 \epsilon_r(x) \tilde{w} = k^2 (\epsilon_r(x) - 1) v \qquad \text{in} \quad \mathbb{R}^2, \tag{21}$$

$$\lim_{r \to \infty} \sqrt{r} \left(\frac{\partial \tilde{w}}{\partial r} - \mathrm{i} k \tilde{w} \right) = 0. \tag{22}$$

Then (20) can be rewritten as

$$\int_D (\Delta \tilde{w} + k^2 \epsilon_r \tilde{w})(\Phi(\cdot; x_0) + u^s(\cdot; x_0)) \, \mathrm{d}x = 0. \tag{23}$$

Using Green's formula, the equation satisfied by $u^s := u^s(\cdot; x_0)$ and the fact that u^s and $\tilde{w}$ are radiating solutions, we obtain

$$\begin{aligned} \int_D (\Delta \tilde{w} + k^2 \epsilon_r \tilde{w}) u^s \, \mathrm{d}x &= \int_D (\Delta u^s + k^2 \epsilon_r u^s) \tilde{w} \, \mathrm{d}x + \int_{\partial D} \left(u^s \frac{\partial \tilde{w}}{\partial \nu} - \tilde{w} \frac{\partial u^s}{\partial \nu} \right) \mathrm{d}s \\ &= k^2 \int_D (\epsilon_r - 1) \Phi(\cdot; x_0) \tilde{w} \, \mathrm{d}x. \end{aligned} \tag{24}$$

On the other hand

$$\int_D \Delta \tilde{w} \Phi(\cdot; x_0) \, \mathrm{d}x = \int_D \Delta \Phi(\cdot; x_0) \tilde{w} \, \mathrm{d}x + \int_D \left(\Phi(\cdot; x_0) \frac{\partial \tilde{w}}{\partial \nu} - \tilde{w} \frac{\partial \Phi(\cdot; x_0)}{\partial \nu} \right) \mathrm{d}s. \tag{25}$$

Substituting (25) and (24) into (23) and using the Green's representation formula in $\mathbb{R}^2 \backslash \overline{D}$ we obtain

$$0 = \int_D \tilde{w} (\Delta \Phi(\cdot; x_0) + k^2 \Phi(\cdot; x_0)) \, \mathrm{d}x + \int_{\partial D} \left(\Phi(\cdot; x_0) \frac{\partial \tilde{w}}{\partial \nu} - \tilde{w} \frac{\partial \Phi(\cdot; x_0)}{\partial \nu} \right) \mathrm{d}s = \tilde{w}(x_0).$$

Hence, $\tilde{w}(x_0) = 0$ for all $x_0 \in \Lambda$ and since $\tilde{w}$ is a radiating solution of the Helmholtz equation outside Λ, we can conclude from the uniqueness of the exterior Dirichlet problem that $\tilde{w} = 0$ outside the domain bounded by Λ. Finally, by the unique continuation principle, we have that $\tilde{w} = 0$ outside D. Hence v and $w =: \tilde{w} + v$ satisfy the homogeneous interior transmission problem (7)–(10). We have shown that any function $v \in \mathbb{H}(\Omega)$ such that $Rv = 0$ is together with $w := \tilde{w} + v$ a solution of the homogeneous interior transmission problem and consequently $v = 0$ if and only if k is not a transmission eigenvalue. This ends the proof. □

Theorem 3.2. *If k is not a transmission eigenvalue, then the reciprocity gap operator $R : \mathbb{H}(\Omega) \to L^2(\Lambda)$ has dense range.*

Proof. Let $\beta \in L^2(\Lambda)$ and assume that

$$(Rv, \beta)_{L^2(\Lambda)} = 0 \qquad \text{for all} \quad v \in \mathbb{H}(\Omega).$$

Then from (18) and (19) and the bi-linearity of $\mathcal{R}$, we have $0 = (Rv, \beta)_{L^2(\Lambda)} = \mathcal{R}(\mathcal{Q}, v)$ where

$$\begin{aligned}\mathcal{Q}(x) &= \int_\Lambda \beta(x_0) u(x; x_0)\, \mathrm{d}s_{x_0} \\ &= \int_\Lambda \beta(x_0 \Phi(x; x_0)\, \mathrm{d}s_{x_0} + \int_\Lambda \beta(x_0) u^s(x; x_0)\, \mathrm{d}s_{x_0}.\end{aligned}$$

Obviously, $\mathcal{Q} = \mathcal{Q}^i + \mathcal{Q}^s$ is the total field satisfying the direct scattering problem

$$\Delta \mathcal{Q}^s + k^2 \epsilon_r \mathcal{Q}^s = k^2(1 - \epsilon_r)\mathcal{Q}^i \qquad \text{in} \quad \mathbb{R}^2$$

and $\mathcal{Q}^s$ satisfies the Sommerfeld radiation condition where

$$\mathcal{Q}^i(x) := \int_\Lambda \beta(x_0)\Phi(x; x_0)\, \mathrm{d}s_{x_0} \qquad \text{and} \qquad \mathcal{Q}^s(x) := \int_\Lambda \beta(x_0) u^s(x; x_0)\, \mathrm{d}s_{x_0}.$$

Hence from Green's formula we have that

$$0 = \mathcal{R}(\mathcal{Q}, v) = k^2 \int_D (\epsilon_r - 1)\mathcal{Q} v\, \mathrm{d}x \qquad \text{for all} \quad v \in \mathbb{H}(\Omega).$$

From the proof of theorem 2.2, the fact that $\mathbb{H}(\Omega)$ contains the space H defined by (13) and the fact that k is not a transmission eigenvalue, we conclude that $\mathcal{Q} = 0$ in D. Hence by the unique continuation principle $\mathcal{Q} = 0$ inside the domain bounded by Λ. Furthermore, since $\mathcal{Q}$ is continuous across Λ, we have that $\mathcal{Q} = 0$ outside Λ from the uniqueness of the exterior Dirichlet problem. Finally, computing the jump of $\mathcal{Q}$ across Λ, we conclude that $\beta = 0$ which proves the theorem. □

If instead of the whole space $\mathbb{H}(\Omega)$ we consider the dense set of $\mathbb{H}(\Omega)$ containing all Herglotz wavefunctions [5]

$$\{v_g \text{ given by (6) for all } g \in L^2(S)\}$$

we can define the *near field* integral operator $\mathcal{N} : L^2(S) \to L^2(\Lambda)$ by $\mathcal{N}g := R(v_g)$. Assuming that $D \backslash \overline{D}_0$ contains the origin we expect that, as in the case of the far field equation described in section 2, the regularized solution $g \in L^2(S)$ of ill-posed integral equation

$$(\mathcal{N}g)(x_0) = \ell(x_0) \qquad x_0 \in \Lambda$$

where $\ell(x_0) := \mathcal{R}(u(\cdot; x_0), \Phi(\cdot, 0))$ will be large if k is a transmission eigenvalue. This provides a method to determine the transmission eigenvalues using near field measured data and point sources as incident fields.

We end this section by remarking that, in contrast to the case of far field data where one considers the far field equation, it is now possible to derive different integral equations

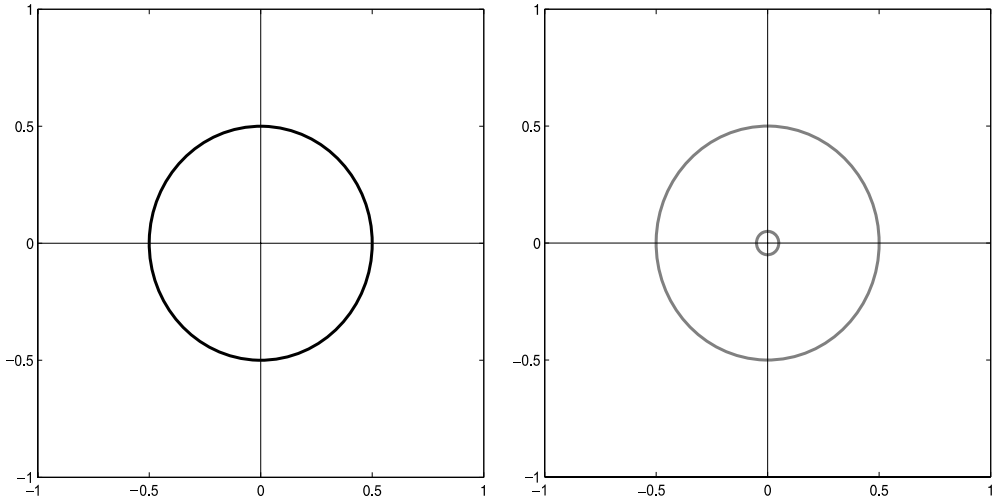

Figure 2. Panel (a) shows the hosting medium D which has the index of refraction $\epsilon_r = 16$. Panel (b) shows the same hosting medium with a cavity D_0. The radius of the cavity is $R_0 = 0.05$.

depending on the choice of dense sets of $\mathbb{H}(\Omega)$. In particular, instead of the set of Herglotz functions, one can use single layer potentials of the form

$$(\mathcal{S}\varphi)(x) := \int_{\tilde{\Lambda}} \varphi(x)\Phi(x, y)\, \mathrm{d}s_y, \qquad \text{for all} \quad \varphi \in L^2(\tilde{\Lambda}),$$

where $\tilde{\Lambda}$ is a closed curve (or part of a closed analytic curve) enclosing Λ inside. In this case the near field operator $\mathcal{N} : L^2(\tilde{\Lambda}) \to L^2(\Lambda)$ is defined by $\mathcal{N}\varphi := R(\mathcal{S}\varphi)$ and the ill-posed integral equation

$$(\mathcal{N}\varphi)(x_0) = \ell(x_0) \qquad x_0 \in \Lambda$$

is solved for φ for a range of wave numbers k. The best choice of the dense set will be examined in a future paper.

Finally, we again emphasize that due to the use of Cauchy data of the total field as measurements the gap reciprocity functional method is not affected by inhomogeneities that may be present in the background outside Ω.

4. Numerical examples

We shall now present some simple numerical tests using the far field pattern as data. This numerical study is preliminary and not comprehensive by any means. Our main goal is to determine in simple simulations if what is suggested from our theoretical investigation actually happens. In particular, we want to answer the following questions: are the transmission eigenvalues retrievable from the far field data? Do transmission eigenvalues shift to the right if voids are present in the hosting medium and if so how does this shift depend on the size and the position of the void? What happens in the case of limited aperture data? Note that the theory developed in section 2 suggests answers to the above questions but does not resolve them.

We use a cubic finite element code to compute the far field pattern $u_\infty(\hat{x}; d, k)$ of a given scatterer for many incident directions d and observation directions $\hat{x}$ (more precisely,

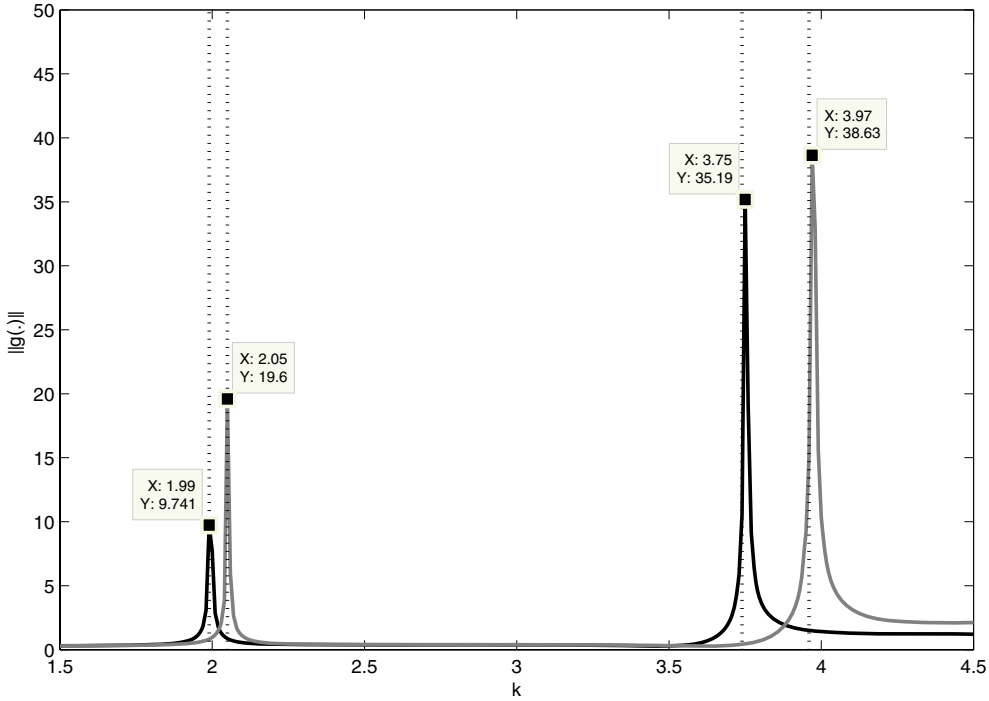

Figure 3. The transmission eigenvalues detected from the far field pattern for geometries shown in figure 2. Both plots show a graph of $\|g\|_{L^2(\Omega)}$ against k; the black plot corresponds to the disk without any cavity shown in figure 2(a) whereas the gray plot corresponds to the disk with the cavity shown in figure 2(b). The peaks are good candidates for the first and second eigenvalues in both cases. This claim is confirmed using the exact values determined by the determinant criteria (27) and (28) marked as dashed lines.

60 directions for each k uniformly distributed on the unit circle) and a range of wave numbers k. The same finite element grid is used for all wave numbers (the grid is suitable for the highest wave number) and a perfectly matched layer (PML) of fixed width and parameters is used to truncate the domain. This limits the range of wave numbers at the top (grid size) and bottom (PML accuracy). Once the approximate far field pattern is known (with roughly 1% noise added as in [3]) we can solve the far field equation

$$\int_S u_\infty(\hat{x}; d, k) g(d)\, \mathrm{d}s_d = 1 \qquad \hat{x} \in S \tag{26}$$

using Tikhonov regularization and the Morozov discrepancy principle as in [3] for each wave number, and try to determine the transmission eigenvalues from peaks in a graph of the L^2 norm of g against k. We then compare the transmission eigenvalues corresponding to a given D and ϵ_r for $D_0 = \emptyset$ with those of the same D and ϵ_r with a cavity D_0 inside.

In our first example the host medium D is the disk of radius $R = 0.5$ centered at the origin with index of refraction $\epsilon_r = 16$ and the void D_0 is the concentric disk of radius $R_0 = 0.05$ as shown in figure 2. This example allows us to compare analytically computed transmission eigenvalues with the results of numerical experiments and verify that the procedure works in this special case. For the homogeneous disk with radius R constant ϵ_r the transmission

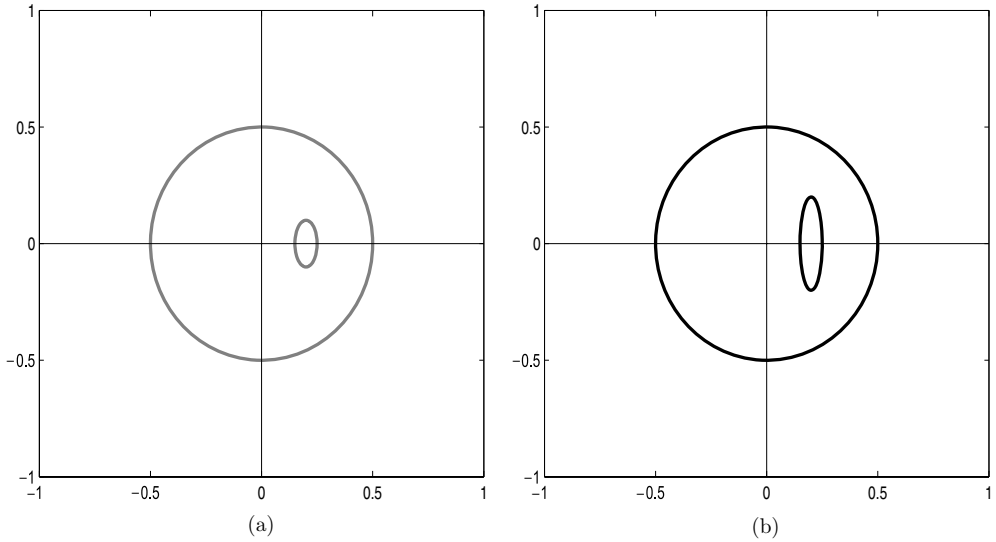

Figure 4. The hosting medium is the disk centered at the origin with radius 0.5 and $\epsilon_r = 16$. In the left panel we show D with the cavity D_0 the ellipse with the axis $a = 0.05$, $b = 0.1$ centered at $(0.2, 0)$. In the right panel we show D with the cavity D_0 the ellipse with the axis $a = 0.05$, $b = 0.2$ centered at $(0.2, 0)$

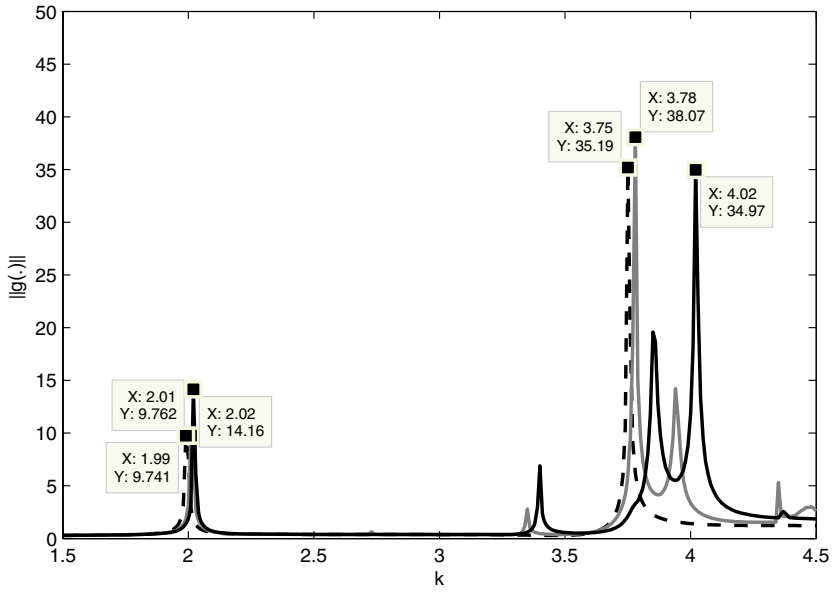

Figure 5. Here we show the plot of $\|g\|_{L^2(S)}$ against k for the obstacles shown in figure 4: black dashed line corresponds to circle without cavity shown in figure 2(a), gray solid line corresponds to the circle with the cavity the small ellipse shown in figure 4(a) and black solid line corresponds to the circle with the cavity the larger ellipse shown in figure 4(b)

eigenvalues are the positive value of k^2 for which (see [7])

$$\det \begin{pmatrix} J_0(kR) & J_0(k\sqrt{\epsilon_r}R) \\ -J_1(kR) & -\sqrt{\epsilon_r}J_1(k\sqrt{\epsilon_r}R) \end{pmatrix} = 0. \tag{27}$$

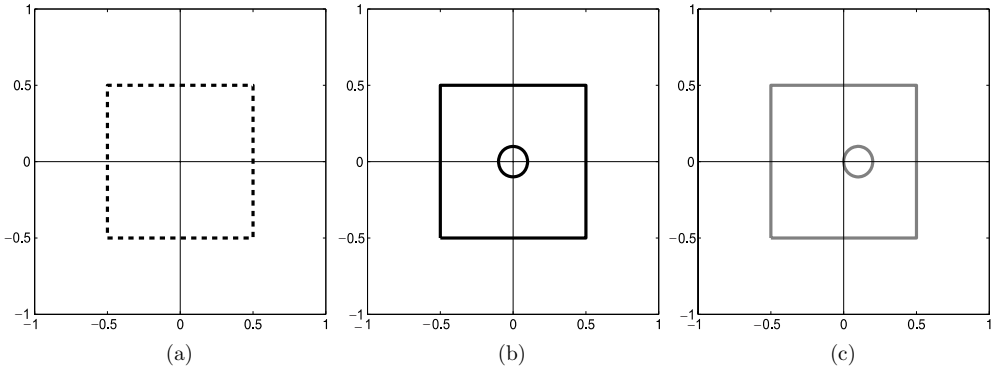

Figure 6. Panel (a) shows the tested medium which is a dielectric with $\epsilon_r = 16$. Panels (b) and (c) show the medium of panel (a) with a void presented by the inner disk. Both voids are of radius 0.1.

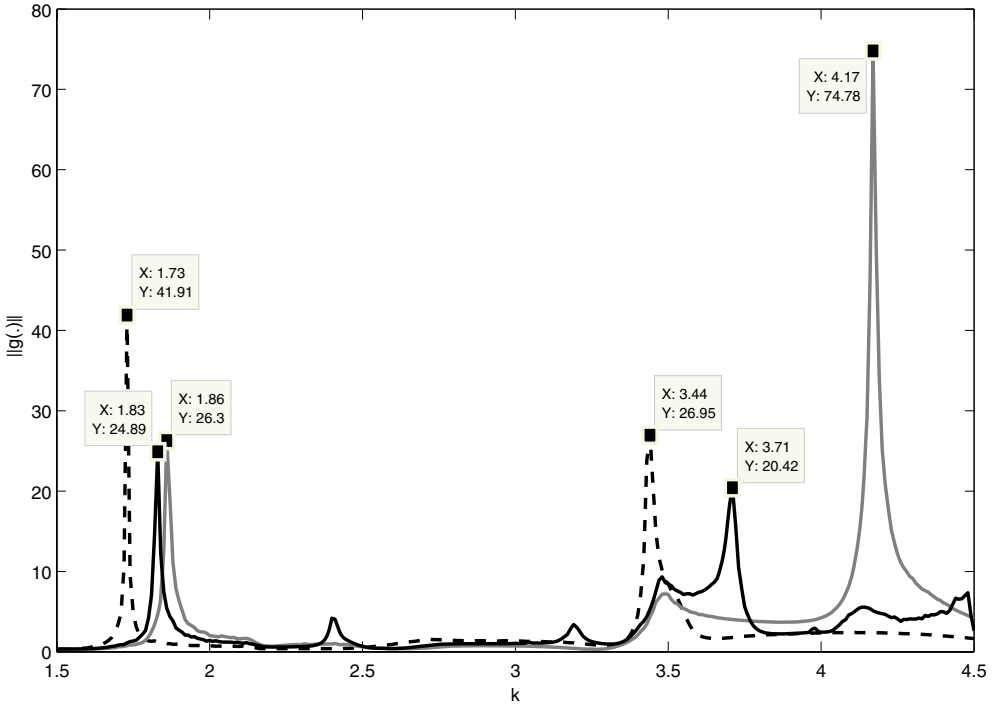

Figure 7. Here we show the plot of $\|g\|_{L^2(S)}$ against k for the obstacles shown in figure 6: black dashed line corresponds to square without cavity shown in figure 6(a), black solid line corresponds to the square with the cavity the circle centered at the origin shown in figure 6(b) and gray solid line corresponds to the square with the cavity the circle centered at $(0.1, 0)$ shown in figure 6(c).

When $\epsilon_r = 16$ and $R = 0.5$ this gives an estimate for the first and second transmission eigenvalues $k_0 = 1.99$ and $k_1 = 3.74$, respectively. If there is a concentric circular cavity with radius $R_0 < R$ then the transmission eigenvalues are the positive values of k^2 for which

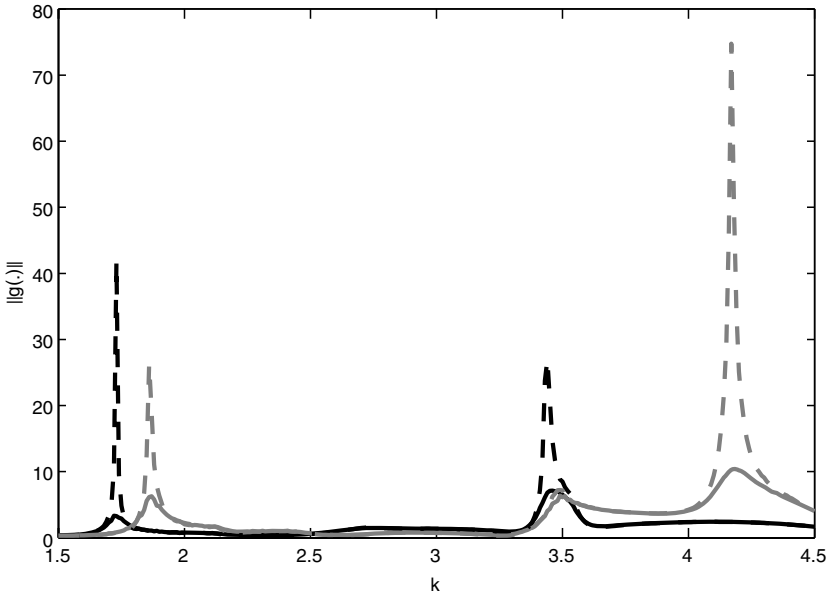

Figure 8. Here we plot $\|g\|_{L^2(S)}$ against k for obstacle of the shapes shown in figures 6(a) and (b) for complex-valued index of refraction $\epsilon_r = 16 + \frac{i}{k}$ and real-valued index of refraction $\epsilon_r = 16$. Black dashed line corresponds to the square shown in figure 6(a) with $\epsilon_r = 16$ whereas black solid line corresponds to the same obstacle with $\epsilon_r = 16 + \frac{i}{k}$. Similarly, gray dashed line corresponds to the square shown in figure 6(b) with $\epsilon_r = 16$ whereas gray solid line corresponds to the same obstacle with $\epsilon_r = 16 + \frac{i}{k}$.

$$\det \begin{pmatrix} J_0(kR_0) & -J_0(k\sqrt{\epsilon_r}R_0) & -H_0(k\sqrt{\epsilon_r}R_0) & 0 \\ -J_1(kR_0) & \sqrt{\epsilon_r}J_1(k\sqrt{\epsilon_r}R_0) & \sqrt{\epsilon_r}H_1(k\sqrt{\epsilon_r}R_0) & 0 \\ 0 & -J_0(k\sqrt{\epsilon_r}R) & -H_0(k\sqrt{\epsilon_r}R) & J_0(kR) \\ 0 & \sqrt{\epsilon_r}J_1(k\sqrt{\epsilon_r}R) & \sqrt{\epsilon_r}H_1(k\sqrt{\epsilon_r}R) & -J_1(kR) \end{pmatrix} = 0. \tag{28}$$

When $\epsilon_r = 16$, $R = 0.5$ and $R_0 = 0.05$ this gives an estimate for the first and second transmission eigenvalues $k_0 = 2.05$ and $k_1 = 3.96$, respectively. These eigenvalues are marked in figure 3 as dashed lines. In figure 3 we show a plot of $\|g\|_{L^2(S)}$ against k where g, the approximate regularized solution of (26), is computed as described above for 201 wave numbers equally distributed in $[0.5, 4.5]$ (data from the finite element solver is used). It is clear that candidates for transmission eigenvalues are visible as peaks in the plot. We also superimpose the true value of k. The match between the eigenvalues computed by the far field pattern and the exact values is very good. The black plot corresponds to the disk without the cavity and the gray plot corresponds to the same disk with the cavity. This example shows that the far field equation (26) in principle provides a means of detecting the transmission eigenvalues. This example also shows that the transmission eigenvalues are shifted to the right if a cavity is present and the shift is larger for the second eigenvalue. Note that the size void for this example is very small.

The next example is for the configurations shown in figure 4. The host medium is the same as for the previous example, i.e. the disk shown in 2(a). The cavities are ellipses with the axis $a = 0.05, b = 0.1$ (figure 4(a)) and $a = 0.05$ and $b = 0.2$ (figure 4(b)) both centered at the point $(0.2, 0)$. The far field patterns for both cases are again computed using the finite element method. The results are shown in figure 5 where we plot the L^2 norm of the regularized solution of the far field equation (26) for three domains: the disk D without cavity (shown by

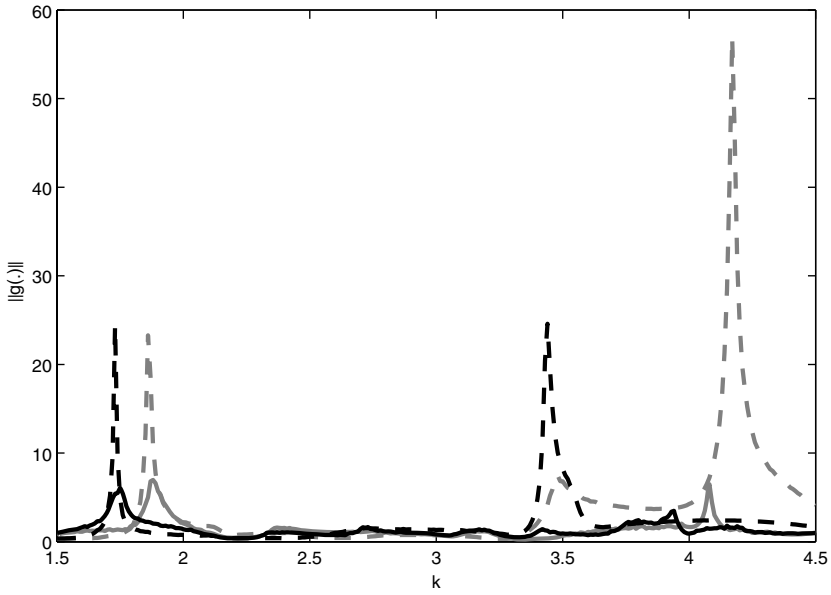

Figure 9. Here we show the transmission eigenvalues for the objects in figures 6(a) and (b) with $\epsilon_r = 16 + \frac{i}{10k}$ for limited aperture data and compare the results for the same scatterers with full aperture data. The graphs in black correspond to the square without void (shown in figure 6(a)); dashed black line with full aperture data whereas solid black line with limited aperture data. The graphs in gray correspond to the square with the void (shown in 6(b)); dashed gray line with full aperture data whereas solid gray line with limited aperture data. In the case of limited aperture data we have $d, -\hat{x} \in [0, \pi]$. In this case we observe that, although the profile of the transmission eigenvalues changes with the aperture of data, it is still possible to distinguish between the medium without and with a void.

dashed line), D with the cavity the small ellipse in figure 4(a) (shown by the black solid line) and D with the cavity the bigger ellipse in figure 4(b) (shown by the gray solid line). The transmission eigenvalues are again shifted to the right if voids are present and the larger the void is the bigger the shifting. However, for this example the shifting of the first transmission eigenvalue is very small and probably not reliable to detect cavities. The shifting of the second transmission eigenvalue is more visible especially for the larger cavity. In both cases in this example the cavities are still of relatively small size. As the next example shows the shifting of the first eigenvalue is more significant for larger voids. However our results suggest that it is better to look for larger transmission eigenvalues. We remark that in our computations the range of k is limited by our ability to compute the simulated data which does not present a problem in practice since data can be measured for a large range of frequencies.

Our third example is the square $[-0.50.5] \times [-0.50.5]$ shown in figure 6(a) with $\epsilon_r = 16$. We consider two cases: the square with a circular cavity centered at the origin of radius 0.1 shown in figure 6(b) and the square with circular cavity of radius 0.1 centered at $(0.1, 0)$ shown in figure 6(c). The corresponding plots of $\|g\|_{L^2(S)}$ where g is the regularized solution of the far field equation (26) are shown in figure 7. The results presented in figure 7 show that the shifting to the right of the transmission eigenvalues is more prominent for voids of bigger size as compared to the example of figure 5. The position of the cavities of the same size changes the profile of the plot, in particular the location of higher eigenvalues, but nevertheless the eigenvalues corresponding to the medium with cavity are always shifted to the right.

Although not covered by our theory (transmission eigenvalues do not exist if $\mathrm{Im}(\epsilon_r) > 0$ in a small ball in D [7]), it is interesting to consider how absorption affects the algorithm. In figure 8 we plot the norm of g against k when $\epsilon_r = 16 + \frac{\mathrm{i}}{k}$ using data from the finite element solver for the obstacles in figures 6(a) and (b). We superimpose these plots with those for the same obstacles but with real index of refraction $\epsilon_r = 16$. We observe that the peaks for the absorbing medium are decreased in amplitude but they occur for the same values of k. In particular, the transmission eigenvalues are clearly visible suggesting that the algorithm can potentially be used in detecting cavities inside a low absorbing medium.

Our final test is to use limited aperture data. We now solve the far field equation

$$\int_{S_0} u_\infty(\hat{x}; d, k) g(d)\, \mathrm{d}s_d = 1 \qquad -\hat{x} \in S_0,$$

where S_0 is now part of the unit circle. Typically, since the approximation of v satisfying (8) by Herglotz functions with kernel supported on part of the unit sphere deteriorate, we expect that the performance our algorithm worsen with the decrease of the aperture of the far field data. We test this for S_0 the unit half circle corresponding to the polar angle $\theta \in [0, \pi]$ for the obstacles in figures 6(a) and (b) with $\epsilon_r = 16 + \frac{\mathrm{i}}{10k}$. The results are shown in figure 9. We still observe the shift to the right of the transmission eigenvalues if a cavity is present.

5. Conclusions

We have introduced a simple algorithm to detect cavities in dielectrics using multistatic data for a range of frequencies. This algorithm is based on the shifting of transmission eigenvalues if a cavity appears in the medium. It is assumed that the eigenvalues are known for the dielectric medium without the defect. We have shown that the transmission eigenvalues can be computed from the far field data and we expect the same for near field data using the reciprocity gap functional method developed in section 3. However, the case of near field data still needs to be numerically tested. We have also shown that the method is still valid if the host medium is slightly absorbing. An attracting feature of this method is that there is no need to know Green's function of the host medium. The implementation of the method is very fast and simple and both detects the present of a cavity and gives some indication of its size.

The goal of this paper is to introduce our method and show with simple examples its potential use in the non-destructive testing of dielectrics. More numerical tests are needed to establish the viability of the method. This method also suggests many interesting and challenging mathematical questions to be studied. In particular, the question of the existence of the transmission eigenvalues in the presence of cavities and the mathematical justification of the dependence of the transmission eigenvalues on the size of cavities are still open.

Acknowledgments

This work was done while M Çayören was visiting the University of Delaware on a grant from the Scientific and Technological Research Council of Turkey. The hospitality and the support are gratefully acknowledged. The research of F Cakoni and D Colton is supported in part by the US Air Force Office of Scientific Research under grant FA9550-05-1-0127. The authors thank Peter Monk for providing the finite element code for solving the direct scattering problem.

References

[1] Cakoni F, Colton D and Monk P 2007 On the use of transmission eigenvalues to estimate the index of refraction from far field data *Inverse Problems* **23** 507–22

[2] Cakoni F, Fares MB and Haddar H 2006 Analysis of two linear sampling methods applied to electromagnetic imagining of burried objects *Inverse Problems* **22** 845–67

[3] Colton D, Coyle J and Monk P 2000 Recent developments in inverse acoustic scattering theory *SIAM Rev.* **42** 369–414

[4] Colton D and Haddar H 2005 An application of the reciprocity gap functional to inverse scattering theory *Inverse Problems* **21** 383–98

[5] Colton D and Kress R 2001 On the denseness of Herglotz wavefunctions and electromagnetic Herglotz pairs in Sobolev spaces *Math. Methods Appl. Sci.* **24** 1289–303

[6] Colton D and Kress R 1998 *Inverse Acoustic and Electromagnetic Scattering Theory* 2nd edn (Berlin: Springer)

[7] Colton D, Päivärinta P and Sylvester J 2007 The interior transmission problem *Inverse Problems Imaging* **1** 13–28

[8] Päivärinta P and Sylvester J Transmission eigenvalues *SIAM J. Math. Anal.* **40** 738–53

[9] Sylvester J An estimate for the free Helmholtz equation that scales at press